

# Ion energy distributions in highly transient EUV induced plasma in hydrogen

**Citation for published version (APA):**

van de Ven, T. H. M., Reefman, P., de Meijere, C. A., van der Horst, R. M., van Kampen, M., Banine, V. Y., & Beckers, J. (2018). Ion energy distributions in highly transient EUV induced plasma in hydrogen. *Journal of Applied Physics*, 123(6), 1-6. [063301]. <https://doi.org/10.1063/1.5017303>

**DOI:**

[10.1063/1.5017303](https://doi.org/10.1063/1.5017303)

**Document status and date:**

Published: 14/02/2018

**Document Version:**

Publisher's PDF, also known as Version of Record (includes final page, issue and volume numbers)

**Please check the document version of this publication:**

- A submitted manuscript is the version of the article upon submission and before peer-review. There can be important differences between the submitted version and the official published version of record. People interested in the research are advised to contact the author for the final version of the publication, or visit the DOI to the publisher's website.
- The final author version and the galley proof are versions of the publication after peer review.
- The final published version features the final layout of the paper including the volume, issue and page numbers.

[Link to publication](#)

**General rights**

Copyright and moral rights for the publications made accessible in the public portal are retained by the authors and/or other copyright owners and it is a condition of accessing publications that users recognise and abide by the legal requirements associated with these rights.

- Users may download and print one copy of any publication from the public portal for the purpose of private study or research.
- You may not further distribute the material or use it for any profit-making activity or commercial gain
- You may freely distribute the URL identifying the publication in the public portal.

If the publication is distributed under the terms of Article 25fa of the Dutch Copyright Act, indicated by the "Taverne" license above, please follow below link for the End User Agreement:

[www.tue.nl/taverne](http://www.tue.nl/taverne)

**Take down policy**

If you believe that this document breaches copyright please contact us at:

[openaccess@tue.nl](mailto:openaccess@tue.nl)

providing details and we will investigate your claim.

## Ion energy distributions in highly transient EUV induced plasma in hydrogen

T. H. M. van de Ven, P. Reefman, C. A. de Meijere, R. M. van der Horst, M. van Kampen, V. Y. Banine, and J. Beckers

Citation: *Journal of Applied Physics* **123**, 063301 (2018); doi: 10.1063/1.5017303

View online: <https://doi.org/10.1063/1.5017303>

View Table of Contents: <http://aip.scitation.org/toc/jap/123/6>

Published by the [American Institute of Physics](#)

---

### Articles you may be interested in

[Optical properties of electrically connected plasmonic nanoantenna dimer arrays](#)

*Journal of Applied Physics* **123**, 063101 (2018); 10.1063/1.5008511

[Effect of shell thickness of gold-silica core-shell nanospheres embedded in an organic buffer matrix for plasmonic solar cells](#)

*Journal of Applied Physics* **123**, 063102 (2018); 10.1063/1.5013329

[Effect of Coulomb collision between surface produced  \$H^-\$  ions and  \$H^+\$  ions on  \$H^-\$  extraction mechanism and beam optics in a Cs-seeded  \$H^-\$  ion source by 3D particle in cell model](#)

*Journal of Applied Physics* **123**, 063302 (2018); 10.1063/1.5004074

[Theory of electromagnetic wave propagation in ferromagnetic Rashba conductor](#)

*Journal of Applied Physics* **123**, 063902 (2018); 10.1063/1.5011130

[Study of magnetization and magnetoelectricity in  \$CoFe\_2O\_4/BiFeO\_3\$  core-shell composites](#)

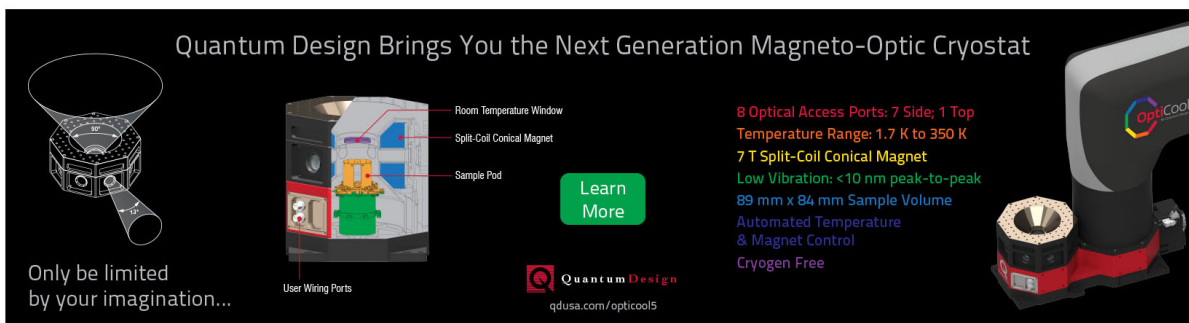
*Journal of Applied Physics* **123**, 064101 (2018); 10.1063/1.5008542

[A novel method to hit the limit temperature of Stirling-type cryocooler](#)

*Journal of Applied Physics* **123**, 063901 (2018); 10.1063/1.5013602

---

Quantum Design Brings You the Next Generation Magneto-Optic Cryostat



Only be limited by your imagination...

Learn More

Quantum Design  
qdusa.com/opticool5

8 Optical Access Ports: 7 Side; 1 Top  
Temperature Range: 1.7 K to 350 K  
7 T Split-Coil Conical Magnet  
Low Vibration: <10 nm peak-to-peak  
89 mm x 84 mm Sample Volume  
Automated Temperature & Magnet Control  
Cryogen Free

# Ion energy distributions in highly transient EUV induced plasma in hydrogen

T. H. M. van de Ven,<sup>1</sup> P. Reefman,<sup>1</sup> C. A. de Meijere,<sup>2</sup> R. M. van der Horst,<sup>2</sup>  
 M. van Kampen,<sup>2</sup> V. Y. Banine,<sup>1,2</sup> and J. Beckers<sup>1,a)</sup>

<sup>1</sup>University of Technology Eindhoven, Eindhoven, The Netherlands

<sup>2</sup>ASML, Veldhoven, The Netherlands

(Received 27 November 2017; accepted 25 January 2018; published online 9 February 2018)

This work reports on the measurements of ion flux composition and ion energy distribution functions (IEDFs) at surfaces in contact with hydrogen plasmas induced by extreme ultraviolet (EUV) radiation. This special type of plasma is gaining interest from industries because of its appearance in extreme ultraviolet lithography tools, where it affects exposed surfaces. The studied plasma is induced in 5 Pa hydrogen gas by irradiating the gas with short (30 ns) pulses of EUV radiation ( $\lambda = 10\text{--}20\text{ nm}$ ). Due to the low duty cycle ( $10^{-4}$ ), the plasma is highly transient. The composition and IEDF are measured using an energy resolved ion mass spectrometer. The total ion flux consists of  $\text{H}^+$ ,  $\text{H}_2^+$ , and  $\text{H}_3^+$ .  $\text{H}_3^+$  is the dominant ion as a result of the efficient conversion of  $\text{H}_2^+$  to  $\text{H}_3^+$  upon collision with background hydrogen molecules. The IEDFs of  $\text{H}_2^+$  and  $\text{H}_3^+$  appear similar, showing a broad distribution with a cut-off energy at approximately 8 eV. In contrast, the IEDF of  $\text{H}^+$  shows an energetic tail up to 18 eV. Most probably, the ions in this tail gain their energy during their creation process by photoionization and dissociative electron impact ionization. Published by AIP Publishing. <https://doi.org/10.1063/1.5017303>

## I. INTRODUCTION

Photon induced plasmas differ from most human-made plasmas (inductively or capacitively coupled plasmas, dielectric barrier discharges, and coronas), in that there is no external electric field acceleration of the electrons that supplies energy to sustain the discharge. Until recently, the experimental research into photon induced plasmas has been scarce due to the lack of industrial applications. In nature, the presence of photon induced plasmas is widespread in the interstellar medium, where they are found in the form of H II regions and planetary nebulae.<sup>1,2</sup>

Recently, photon induced plasmas attracted attention from the semiconductor industry because these plasmas are inevitably present in the latest generation lithography tools. For the sake of shrinking transistor sizes, extreme ultraviolet (EUV) lithography has been introduced, which uses a much shorter illumination wavelength (13.5 nm) than the previous, deep ultraviolet systems (193 nm).<sup>3</sup> The used EUV radiation ionizes the low pressure (typically 1–10 Pa) background gas, inevitably present in the lithography tools, creating plasma as a by-product.<sup>4–6</sup>

In EUV lithography, multilayer mirrors are used for the imaging and transport of EUV radiation. In the field, these mirrors should retain their reflectivity under EUV irradiation, which is non trivial due to the high absorption of EUV radiation by even a small amount of contamination [a carbon layer only 15 Å thick reduces the mirror reflectivity by 2% (Ref. 7)]. The processes that influence the reflectivity are actively investigated in multiple studies.<sup>5,7–15</sup>

The interaction between EUV induced plasma and adjacent surfaces can have beneficial effects such as the removal of contamination by EUV-reactive ion sputtering.<sup>5</sup> Negative effects include the degradation of multilayer coatings due to

delamination leading to the formation of blisters.<sup>10,16</sup> This phenomenon has been attributed to impact by high energy hydrogen ions formed in the plasma and accelerated by plasma-induced electric fields. Blister formation in Mo/Si multilayer samples due to ion irradiation has been confirmed experimentally using moderate energy (50–200 eV)<sup>15</sup> and energetic (>800 eV) hydrogen ions.<sup>13,17</sup> Even deuterium ions with energies as low as 5 eV have been shown to be capable of having a negative influence on EUV lithography relevant optical materials.<sup>11</sup>

Some of these studies<sup>10,11,13,15</sup> relate their work to mirror degradation in EUV lithography by suggesting that the used ion sources serve as a proxy for the ion fluxes created by an EUV induced plasma. The applicability of the used ion sources, in terms of ionic species composition and ion energy distribution function (IEDF), is unclear because these properties have not yet been determined in EUV induced plasma.

To extend the knowledge base to the necessary level, in the present study, the ion fluxes towards surfaces adjacent to EUV induced hydrogen plasma are investigated experimentally using an ion mass spectrometer. Hydrogen gas at 5 Pa is irradiated with pulses of EUV photons with wavelengths closely distributed around 13.5 nm. Although EUV lithography light sources will operate at a very high repetition rate of tens of kHz,<sup>18</sup> in this study, a much lower frequency is used to gain understanding of the basic physical mechanisms. Other research groups have estimated local plasma ion densities using Langmuir probes<sup>19</sup> and ion surfaces fluxes have been characterized using retarding field energy analyzers.<sup>20</sup> Both however lack the ability to resolve individual species. The use of an ion mass spectrometer adds the mass separation and a much larger dynamic range.

Recently, the evolution of pulsed EUV plasmas has been investigated non-intrusively using microwave cavity

<sup>a)</sup>j.beckers@tue.nl

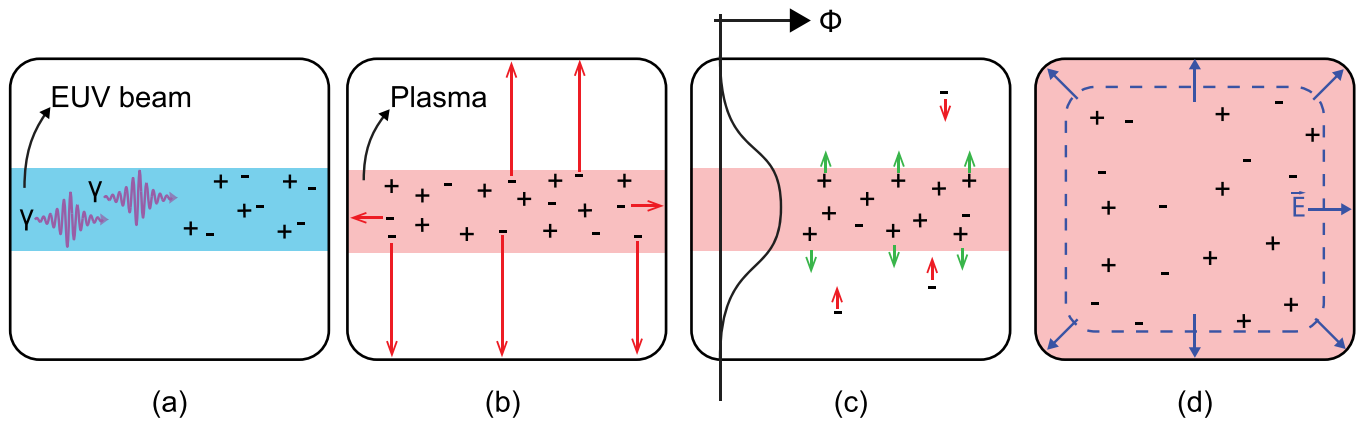


FIG. 1. Illustration of the EUV induced plasma creation and evolution. The image border represents the wall of the experimental geometry. (a) Photoionization creates fast electrons. (b) Fast electrons escape to the wall, leaving behind a positive space charge. (c) The hereby created potential well confines the remaining electrons and accelerates ions outwards. (d) Plasma has fully expanded. The plasma induced electric fields are indicated.

resonance spectroscopy (MCRS)<sup>21,22</sup> and a particle-in-cell (PIC) model.<sup>23,24</sup> When the EUV pulse repetition time is much longer than the plasma decay time, the processes in plasma creation and decay are as follows (also illustrated in Fig. 1):

- Plasma creation is initiated by direct photoionization of the hydrogen gas (ionization energy of 15.6 eV) by the EUV photons ( $h\nu = 60\text{--}125$  eV).
- Due to momentum conservation, most of the excess photon energy is carried by energetic electrons with a highly non-Maxwellian energy distribution. Part of these electrons escape to the wall, leaving behind a positive space charge. The electron mean free path ( $\sim 3$  cm) is slightly smaller than the cylinder radius (5 cm). Therefore, more than 16% of the electrons can reach the wall without colliding.
- The space charge created by the loss of only 1.5% of the fast electrons is sufficient to create a potential well that confines the remaining electrons and accelerate positive ions outwards. The trapped electrons lose their energy within a few tens of nanoseconds<sup>25,26</sup> due to ionizing and other inelastic collisions and at the same moment increase the plasma density. After the plasma creation, the local electron density decreases rapidly due to the expansion of the plasma.
- When the plasma has filled the volume and the electrons have reached their equilibrium temperature, the density continues to decrease via ambipolar diffusion followed by wall recombination.

All energy is supplied within a few tens of nanoseconds by the EUV pulse, while it takes up to a few hundred microseconds for the plasma to completely extinguish.<sup>22</sup> This low duty cycle ( $10^{-4}$ ) makes the plasma highly transient.

The IEDF is expected to be determined by the electron temperature  $T_e$ . In a collisionless DC sheath, the ion impact energy is determined by the sheath-presheath to wall potential,  $\Phi_w = -T_e \ln\left(\frac{m_i}{2\pi m_e}\right)^{1/2}$ , and the Bohm energy,  $\frac{T_e}{2}$ , where  $m_i$  and  $m_e$  are the ion and electron mass, respectively.<sup>27</sup> In a hydrogen plasma, where  $\text{H}_3^+$  is expected to be the dominant ion,<sup>2</sup> the expected ion energy is therefore  $3.88 \times T_e$ . As  $T_e$

decreases to room temperature,<sup>26</sup> the ion energy will also decrease. The complex and dynamic processes in the electron cooling make it difficult to predict the behavior of the sheath potential, but it is expected that during a substantial period of the plasma decay, the electron temperature is below 1 eV (Ref. 26) and the resulting IEDF will therefore contain a majority of  $<4$  eV ions.

## II. EXPERIMENTAL SETUP

A schematic of the setup is shown in Fig. 2. Hydrogen gas at 5 Pa is irradiated with pulsed EUV light, produced by a hollow cathode pinch discharge in xenon. The EUV source has previously been described by Van der Horst.<sup>28</sup> The used repetition frequency of the source is 500 Hz and the EUV pulses have a temporal FWHM of about 30 ns. Since this source also produces substantial amounts of UV and VUV, a 50 nm Si:Zr spectral purity filter (SPF) is used which transmits mostly between 10 and 20 nm. The spectrum has been published by Astakhov and Van der Horst.<sup>21,23</sup> 98% of the radiation energy is within the 10 to 20 nm bandwidth. In the past, the transmission of multiple SPFs has been measured to ensure that the transmission is not SPF specific. Uncertainties in the transmission are smaller than 0.8% in the range from 30 to 60 eV and less than 0.25% below 20 eV.

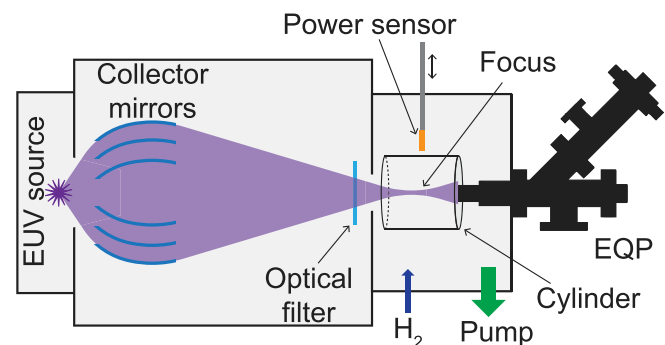


FIG. 2. Sketch of the experimental setup. EUV is generated by the Xe-pinch discharge and focused by collector mirrors into the measuring vessel. The EUV power can be measured with the retractable power sensor. The cylinder is indicated with the EQP placed at the back. EUV is therefore directly incident upon the sample orifice.

The uncertainty in the spectrum before the SPF is larger, because electrode wear could alter the spectral output. The use of the SPF reduces the impact of these variations.

The EUV radiation is focused into the measuring vessel using grazing incidence mirrors. The width at beam waist is 4 mm and the divergence is  $10^\circ$ . The EUV pulse energy is measured before and after each measurement using a calorimetric power sensor, which has also been described by Van der Horst.<sup>28</sup> The pulse energy is  $124 \pm 3 \mu\text{J}$ .

In the preparation of future numerical modeling and to facilitate data analysis, the measuring area is enclosed in an aluminum cylinder that creates a well defined symmetrical geometry. The length and radius are 100 mm and 50 mm, respectively. Due to the divergence of the EUV beam, the beam diameter at the measurement location is almost 38 mm. The EUV energy density is therefore  $157 \pm 4 \text{ mJ/m}^2/\text{pulse}$ . This is of the same order or magnitude as delivered by the current and future EUV sources in EUV lithography irradiating a mirror area of  $0.1 \text{ m}^2$ . Although these sources have a much higher output power of 125–500 W, they operate at a substantially higher frequency of 50 kHz and therefore have a relatively little power per pulse.<sup>18</sup>

The ion flux is measured with an Electrostatic Quadrupole Plasma analyzer (EQP1000, Hiden Analytical Ltd.), an ion mass spectrometer enabling mass and energy resolved measurements. The grounded sampling surface of the EQP is placed perpendicular to the EUV beam at the back plate of the cylinder and is thus directly exposed. All the walls are grounded.

The EQP consists of a sample plate, ion guiding electrostatic lenses, energy filter, quadrupole mass filter, and a secondary electron multiplier ion detector. An extensive description is given in Refs. 29 and 30. The bandwidth of the energy filter is 0.6 eV (FWHM). The EQP has a narrow acceptance angle. It therefore measures the ion velocity distribution in the forward direction,<sup>30</sup> which will be presented in units of energy. Correct operation and interpretation of the measurement results is far from straightforward. We will highlight some of the most important considerations and measures taken to ensure a proper measurement.

To ensure that the plasma is not influenced by the presence of the sample orifice, it should be smaller than the Debye length, which is the distance scale over which electrostatic effects are screened in the plasma. Furthermore, this prevents the plasma from penetrating the EQP, which would disturb the electrostatic fields inside the mass spectrometer which in turn would perturb the measurement of the IEDF. Experimentally, this is manifested as a significant reduction of the  $<2.5 \text{ eV}$  ion flux, which is instead detected with an apparent negative energy.

The smallest Debye length is estimated using an electron temperature of 1 eV and a peak density of  $3 \times 10^{16} \text{ m}^{-3}$  measured with MCRS,<sup>22</sup> which was translated from the electric field averaged electron density to the actual density.<sup>26</sup> The resulting Debye length is  $43 \mu\text{m}$ . Using a  $50 \mu\text{m}$  orifice, a substantial amount of negative ions were detected together with a 20 times reduction in the  $\text{H}_3^+$  flux below 1 eV. Therefore, a sample orifice with a diameter of  $20 \mu\text{m}$  is used that guarantees that plasma does not penetrate the

spectrometer. Using this orifice, no ions with apparent negative energy were measured.

Long term EUV exposure can result in the contamination of the sample plate, which forms a non-conducting layer. The cap is then no longer electrically grounded but floating, which changes the IEDF considerably. Therefore, a fresh and clean plate was used during these measurements. A 50 nm thick ruthenium coating was applied to prevent contamination and oxidation.

The EQP contains electrostatic lenses composed of multiple electrodes which are adjustable by the user. In principle, there are little restrictions regarding the choice of electrode potentials. These settings influence the transmission and the angle under which ions are detected.<sup>29,31</sup> The most important requirement that we have applied here is that no stray ions, at random angles larger than the acceptance angle, should be able to enter the energy filter, as this may cause transmission spikes in the energy spectrum. The SIMION software package<sup>32</sup> was used to simulate the ion trajectories through the device and to find settings that guarantee the fulfillment of the above requirement. The acceptance angle using this settings decreases from  $5^\circ$  at 1 eV to a constant  $1^\circ$  above 10 eV.

The transmission of the mass filter is almost flat with the ion mass, which was determined using appearance potential mass spectrometry (APMS).<sup>33</sup> The measured fluxes of ion species with different mass can therefore be directly compared without the need for mass dependent corrections.

### III. RESULTS AND DISCUSSION

Figure 3 presents the measured IEDFs of hydrogen ions in 5 Pa hydrogen gas. Two observations are made. First, the three species detected are  $\text{H}^+$ ,  $\text{H}_2^+$ , and  $\text{H}_3^+$  ( $m/z = 1, 2,$  and  $3$ ). Mass scans at 4 eV show that no other ions are present. Second, the shapes of the IEDFs of  $\text{H}_2^+$  and  $\text{H}_3^+$  are similar, showing a broad distribution with a steep decrease at about 8–9 eV. The shape of the IEDF of  $\text{H}^+$  in this energy range is similar to that of the other species. However, this distribution

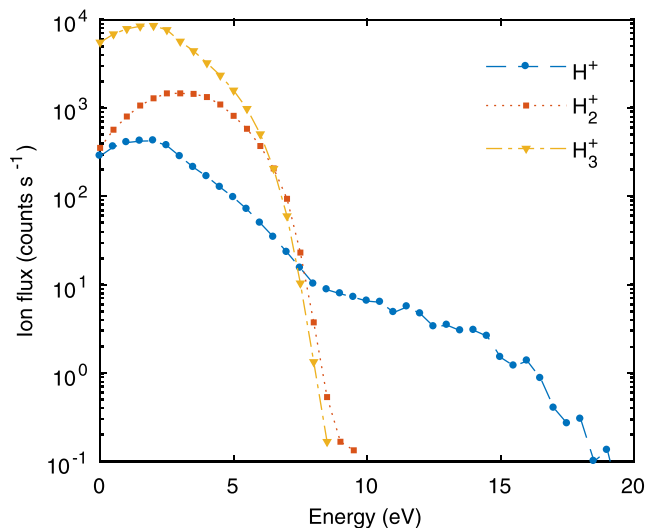


FIG. 3. The species resolved IEDF in EUV induced plasma in 5 Pa hydrogen gas. The EUV pulse energy was  $124 \pm 3 \mu\text{J}$ .

has an energetic tail that extends to just under 20 eV, which was not anticipated.

The influence of ion-molecule collisions is expected to be minor. The ion mean free path is in the order of 1 cm, which is larger than the sheath width, which is typically a few times the Debye length.<sup>27</sup> From the moment of maximum plasma density [ $\sim 10^{16} \text{ m}^{-3}$  (Refs. 22 and 26)], until the density has dropped to  $1 \times 10^{14} \text{ m}^{-3}$ , the Debye length is smaller than 2 mm for  $T_e$  below 5 eV. Because the density has dropped by a factor 100, we also expect that we have captured  $\sim 99\%$  of the total flux. During this period, the Debye length is much shorter than the mean free path and therefore ion-molecule collisions are negligible.

### A. Ion flux composition

The measured  $\text{H}^+$  and  $\text{H}_2^+$  are created by photoionization in a ratio  $\text{H}^+/\text{H}_2^+$  of about 0.27.<sup>34</sup> The excess energy results in the creation of relatively energetic electrons, with energies up to 76 eV. These electrons further ionize the background gas by electron impact ionization, creating mainly  $\text{H}_2^+$  as the cross section for ionization to  $\text{H}_2^+$  is 10 times larger than that for ionization to  $\text{H}^+$ .<sup>35</sup> Hence, more  $\text{H}_2^+$  than  $\text{H}^+$  is created.

Although not created by photo- or electron impact ionization,  $\text{H}_3^+$  appears clearly as the dominant ion. The reason for this is that  $\text{H}_2^+$  is rapidly (0.2  $\mu\text{s}$ ) converted to  $\text{H}_3^+$  by collisions with the background  $\text{H}_2$  gas ( $\text{H}_2^+ + \text{H}_2 \rightarrow \text{H}_3^+ + \text{H}$ ).<sup>36</sup> The dominance of  $\text{H}_3^+$  has been shown in other weakly ionized plasmas,<sup>2</sup> but is now, for the first time, also observed in a photon induced plasma.

### B. Energetic tail

The creation of the high energy tail in  $\text{H}^+$  may be explained by the following two mechanisms:

1. Due to its lower mass,  $\text{H}^+$  is affected more by the temporally high potential.
2. Upon entering the space charge region,  $\text{H}^+$  already has a higher energy than  $\text{H}_2^+$  and  $\text{H}_3^+$  when it enters the space charge region.

In the first mechanism, the observed tail is the result of the lower inertia of  $\text{H}^+$ , compared to that of  $\text{H}_2^+$  and  $\text{H}_3^+$ . The potential peaks shortly after the EUV pulse and then decays within a few tens of nanoseconds because the electrons cool due to electron neutral collisions. All ionic species are accelerated by the resulting electric fields  $\vec{E}$  with the same force due to their equal (single) charge

$$\vec{a}_i(t) = \frac{\vec{F}_i(t)}{m_i} = \frac{q_i \vec{E}(t)}{m_i}, \quad (1)$$

with  $a_i$  and  $\vec{F}_i$ , respectively, being the acceleration and force on species  $i$  and  $m_i$  the particle's mass.

However, assuming that the potential drop decreases significantly over the ion transit time through the sheath, there is only a limited time of fast acceleration.  $\text{H}^+$  gets accelerated to a higher extent than  $\text{H}_2^+$  and  $\text{H}_3^+$  due to its lower mass.

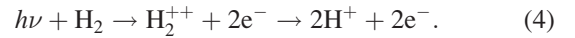
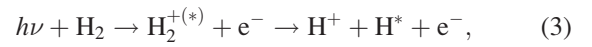
The kinetic energy  $\varepsilon_i$  gained up to  $t = \tau$  is

$$\begin{aligned} \varepsilon_i(t) &= \frac{1}{2} m_i v_i(t)^2 = \frac{m_i}{2} \left[ \int_0^\tau a_i(t) dt \right]^2 \\ &= \frac{q^2}{2m_i} \left[ \int_0^\tau E(t) dt \right]^2. \end{aligned} \quad (2)$$

The ratio of  $\varepsilon(t)$  between species  $i$  and  $j$  is a constant ratio between their masses:  $(\varepsilon_i/\varepsilon_j)(t) = m_j/m_i$ . Therefore,  $\text{H}^+$  gains two times more energy than  $\text{H}_2^+$  and even three times more than  $\text{H}_3^+$  which could result in the formation of a high energy tail.

Following this reasoning, the difference in mass between  $\text{H}_2^+$  and  $\text{H}_3^+$  would also result in a disparity in maximum energy between those species. This is not seen in the present measurements:  $\text{H}_2^+$  and  $\text{H}_3^+$  have the same maximum energy of about 8–9 eV (see Fig. 3). It could be that this is overshadowed by the bulk of the ion flux, but it is nevertheless detrimental to the hypothesis.

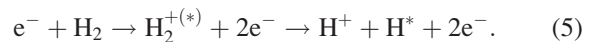
The second mechanism is that  $\text{H}^+$  already has a higher kinetic energy before it is accelerated in the induced space charge. Energetic  $\text{H}^+$  is formed by both dissociative photoionization [Eq. (3)], double photoionization followed by dissociation [Eq. (4)] (Ref. 37), and dissociative electron impact ionization. We first consider the photoionization reactions



In the first process, initially, a repulsive  $^2\Sigma_u^+$  state or an excited molecular ion is formed in a vertical process. Upon dissociation, an  $\text{H}^+$  ion and a hydrogen atom in the excited state are produced. The kinetic energy of the two products depends on the initial state of  $\text{H}_2^{+*}$  and the resulting  $\text{H}^*$ , but is in the order of 8 eV.<sup>37</sup> In the second process, both electrons are removed from the hydrogen molecule to create unstable  $\text{H}_2^{++}$ , which dissociates into two  $\text{H}^+$ . The excess potential energy associated with  $\text{H}_2^{++}$  of 18.8 eV is evenly distributed over the separated  $\text{H}^+$  due to momentum conservation.<sup>38</sup> The resulting ion energy is 9.4 eV.

If we consider the cross sections for ionization, we see that the contribution of dissociative photoionization ( $\sigma(\text{H}^+, \text{H}) = 1.4 \times 10^{-20} \text{ cm}^2$ )<sup>34</sup> to the energetic tail is a few times larger than that of double photoionization ( $\sigma(\text{H}^+, \text{H}^+) = 0.27 \times 10^{-20} \text{ cm}^2$ ),<sup>39</sup> considering that two ions are created in the later process. In photoionization, about 27% of the events lead to the creation of fast  $\text{H}^+$ . About 16% of these ions are created by double photoionization, which is 4.3% of the total photoionization.

Dissociative electron impact ionization involves the same intermediate excited ions as photoionization



In electron impact,  $\text{H}^+$  can be created via the  $^2\Sigma_g^+$  state of  $\text{H}_2^+$  which results in near-zero kinetic energy, or, similar to dissociative photoionization, via the repulsive excited

states of  $\text{H}_2^+$  and the repulsive  ${}^2\Sigma_u^+$  state which result in a broad energy distribution peaked at the energy of  $\sim 8$  eV.<sup>40</sup> Electron impact collisions with energies lower than the threshold of transition to  ${}^2\Sigma_u^+$  mainly result in low energy  $\text{H}^+$  via the  ${}^2\Sigma_g^+$  state. In total, high energy ( $>0.25$  eV)  $\text{H}^+$  is formed in about 5% of the electron impact ionizations.<sup>41</sup> Numerical simulations have shown that at 5 Pa, approximately one electron impact ionization takes place for each photoionization.<sup>23</sup> Therefore, the contribution of dissociative electron impact ionization is roughly equal to that of double photoionization.

Ionization of fast H by electron impact ionization ( $\text{H} + e^- \rightarrow \text{H}^+ + 2e^-, \sigma = 7 \times 10^{-17} \text{cm}^2$ ) can also create energetic  $\text{H}^+$ . However, this cross section is just a factor 10 larger than that of the electron impact ionization of  $\text{H}_2$  to  $\text{H}^+$  and thus the fast H density should be in the order of 10% of the gas density in order for this process to have a substantial contribution. Those fast H are not produced by electron impact ionization and conversion of  $\text{H}_2^+$  to  $\text{H}_3^+$  ( $\text{H}_2^+ + \text{H}_2 \rightarrow \text{H}_3^+ + \text{H}$ ).<sup>2,25</sup> The binary recombination process of  $\text{H}_3^+$  with electrons is negligible at our working pressure<sup>42</sup> and asymmetric charge transfer of  $\text{H}^+$  or  $\text{H}_3^+$  with  $\text{H}_2$  to form fast H requires ions with elevated initial ion energies. Photoionization of  $\text{H}_2$  [Eq. (3)] does create fast H at a rate similar to that of  $\text{H}^+$ . Also, electron impact dissociation creates H ( $\sigma < 9 \times 10^{-17} \text{cm}^2$ ), part of which has energies above 7 eV.<sup>25</sup> The expected rate at which they are created is similar to that of ions. Due to their high velocity, they reach the walls of the vessel within a few  $\mu\text{s}$ , if they have not lost their energy in excitation collisions with the background gas [the mean free path is about 10 mm (Ref. 36)]. Therefore, the fast H will be lost long before the next EUV pulse. The density is therefore not sufficient to contribute to the energetic  $\text{H}^+$  tail. Other energetic  $\text{H}^+$  production processes are negligible because either the ion energy thresholds ( $\text{H}_2^+$  or  $\text{H}_3^+$  dissociation in collision with  $\text{H}_2$  and asymmetric charge transfer between  $\text{H}_2^+$  and H) or molecule kinetic energy thresholds ( $\text{H}_2 + \text{H}_2$  impact ionization) are too high.<sup>2,36</sup>

The energy that ions gain in the above described photo and the electron impact ionization processes match with the length of the energy tail, which extends from 8 to approximately 18 eV. The ions traversing the induced space charge still receive the energy due to the crossing of the space charge region, which is added to their initial energy of approximately 10 eV.

Energetic  $\text{H}^+$  have been measured before in electron impact experiments.<sup>38</sup> Until now, they have not been reported in a plasma experiment. That is because the energy threshold for excitation to a state that produces energetic  $\text{H}^+$  is much larger than the ionization threshold: more than 25 eV for the  $Q_1, {}^1\Sigma_u^+(1)$  state, which autoionizes and dissociates producing  $\text{H}^+$  with energies up to 4.4 eV.<sup>43</sup> Dissociating  $\text{H}_2^*$  states need more than 30 eV to be produced and the vertical threshold for  $\text{H}_2^{++}$  formation is 51.09 eV.<sup>37</sup> Electrons at these energies are scarce in plasmas driven by electric fields. Energetic  $\text{H}^+$  production in laser driven plasmas is also uncommon as laser wavelengths below 50 nm ( $h\nu = 25$  eV) would be required for the ionization via the  $Q_1, {}^1\Sigma_u^+(1)$  state. Therefore, most plasmas lack the mechanisms needed for the production of energetic  $\text{H}^+$ .

## IV. CONCLUSIONS

The current work shows the composition and energy distributions of ions from an EUV induced plasma in  $\text{H}_2$  impacting an electrically grounded surface. This situation is representative for the non-biased mirrors in the imaging part of the EUV lithography tool. It must be noted that these conditions differ from those in the EUV light source part of the tool in terms of pressure, EUV spectrum, pulse frequency, and the presence of tin debris in the form of fast ions, atoms, and particulates.<sup>44</sup> The effects of these differences on the EUV induced plasma and the IEDFs in particular, require further investigation.

The IEDF in EUV induced plasma in hydrogen appears relatively broad with a clear cut-off energy a little under 10 eV. The ion flux consists mainly of  $\text{H}_3^+$ . The energetic tail of  $\text{H}^+$  extends to just under 20 eV.

The observed energies are much lower than the ones used during the investigation of ion induced delamination in multilayer mirrors.<sup>11,13,15</sup> These studies use a thermal gas cracker<sup>11,13</sup> or an ion gun<sup>15</sup> to provide the ion fluxes. Moreover, those devices produce mainly  $\text{H}_2^+$  in contrast to the situation of EUV induced plasma, where also  $\text{H}^+$  and  $\text{H}_3^+$  are present, which could influence the surface chemistry. In bombardment with mono-atomic molecular ions, each atom is usually counted separately.<sup>45</sup> The energy per atom is greatly reduced when  $\text{H}_3^+$  would be used as the beam particle with the same total kinetic energy. Hence, if blistering would be observed close to EUV induced plasma in hydrogen, the mechanisms involved in the blistering formation could be different than the ones investigated in the previous studies.

## ACKNOWLEDGMENTS

The authors would like to thank ASML for their financial support and the experimental time on its EUV sources.

- <sup>1</sup>I. Ridpath, *A Dictionary of Astronomy* (Oxford University Press, 2012).
- <sup>2</sup>T. Oka, "Interstellar  $\text{H}_3^+$ ," *Chem. Rev.* **113**, 8738–8761 (2013).
- <sup>3</sup>E. Sperling, "Moore's Law: A status report," *Semiconductor Engineering* (blog), April 20th, 2017; available at <https://semiengineering.com/moores-law-a-status-report/>.
- <sup>4</sup>M. H. L. van der Velden, W. J. M. Brok, J. J. A. M. van der Mullen, and V. Y. Banine, "Kinetic simulation of an extreme ultraviolet radiation driven plasma near a multilayer mirror," *J. Appl. Phys.* **100**, 073303 (2006).
- <sup>5</sup>A. Dolgov, D. V. Lopaev, T. Rachimova, A. Kovalev, A. Vasil'eva, C. J. Lee, V. M. Krivtsov, O. Yakushev, and F. Bijkerk, "Comparison of  $\text{H}_2$  and He carbon cleaning mechanisms in extreme ultraviolet induced and surface wave discharge plasmas," *J. Phys. D: Appl. Phys.* **47**, 065205 (2014).
- <sup>6</sup>R. M. van der Horst, J. Beckers, S. Nijdam, and G. M. W. Kroesen, "Exploring the temporally resolved electron density evolution in extreme ultra-violet induced plasmas," *J. Phys. D: Appl. Phys.* **47**, 302001 (2014).
- <sup>7</sup>J. Hollenshead and L. Klebanoff, "Modeling radiation-induced carbon contamination of extreme ultraviolet optics," *J. Vac. Sci. Technol., B: Microelectron. Nanometer. Struct. – Process., Meas., Phenom.* **24**, 64 (2006).
- <sup>8</sup>T. E. Madey, N. S. Faradzhev, B. V. Yakshinskiy, and N. V. Edwards, "Surface phenomena related to mirror degradation in extreme ultraviolet (EUV) lithography," *Appl. Surf. Sci.* **253**, 1691–1708 (2006).
- <sup>9</sup>H. Meiling, H. Meijer, V. Banine, R. Moors, R. Groeneveld, H.-J. Voorma, U. Mickan, B. Wolschrijn, B. Mertens, G. van Baars, P. Kürz, and N. Harned, "First performance results of the ASML alpha demo tool," *Proc. SPIE* **6151**, 615108 (2006).

- <sup>10</sup>A. L. Bondareva and G. I. Zmievskaya, "Computer simulation of blistering in multilayer mirrors for EUV lithography," *J. Surf. Invest.: X-ray, Synchrotron Neutron Tech.* **4**, 480–487 (2010).
- <sup>11</sup>A. S. Kuznetsov, R. W. E. Kruijs, M. A. Gleeson, K. Schmid, and F. Bijkerk, "Hydrogen interaction with EUVL-relevant optical materials," *J. Surf. Invest.: X-ray, Synchrotron Neutron Tech.* **4**, 563–566 (2010).
- <sup>12</sup>J. Chen, E. Louis, R. Harmsen, T. Tsarfati, H. Wormeester, M. Van Kampen, W. Van Schaik, R. Van De Kruijs, and F. Bijkerk, "In situ ellipsometry study of atomic hydrogen etching of extreme ultraviolet induced carbon layers," *Appl. Surf. Sci.* **258**, 7–12 (2011).
- <sup>13</sup>A. S. Kuznetsov, M. A. Gleeson, and F. Bijkerk, "Ion effects in hydrogen-induced blistering of Mo/Si multilayers," *J. Appl. Phys.* **114**, 113507 (2013).
- <sup>14</sup>D. I. Astakhov, "Numerical study of extreme-ultra-violet generated plasmas in hydrogen," Ph.D. thesis, University of Twente, Twente, The Netherlands (2016).
- <sup>15</sup>R. A. J. M. van den Bos, C. J. Lee, J. P. H. Benschop, and F. Bijkerk, "Blister formation in Mo/Si multilayered structures induced by hydrogen ions," *J. Phys. D: Appl. Phys.* **50**, 265302 (2017).
- <sup>16</sup>C. Lee, "Enhanced multilayer mirror stability through heterogeneous materials," NWO Domain AES project 13913, [www.stw.nl/nl/content/enhanced-multilayer-mirror-stability-through-heterogeneous-materials](http://www.stw.nl/nl/content/enhanced-multilayer-mirror-stability-through-heterogeneous-materials), accessed July 5th, 2018.
- <sup>17</sup>M. G. Pelizzo, A. J. Corso, P. Zuppella, D. L. Windt, and G. Mattei, "Stability of extreme ultraviolet multilayer coatings to low energy proton bombardment," *Opt. Express* **19**, 14838–14844 (2011).
- <sup>18</sup>I. Fomenkov, "EUVL exposure tools for HVM: Status and outlook," in *2016 International Workshop on EUV Lithography* (ASML, Cymer, San Diego, CA, USA, Berkeley, CA, 2016).
- <sup>19</sup>A. Dolgov, O. Yakushev, A. Abrikosov, E. Snegirev, V. M. Krivtsum, C. J. Lee, and F. Bijkerk, "Extreme ultraviolet (EUV) source and ultra-high vacuum chamber for studying EUV-induced processes," *Plasma Sources Sci. Technol.* **24**, 35003 (2015).
- <sup>20</sup>A. A. Abrikosov, O. F. Yakushev, D. V. Lopaev, and V. M. Krivtsum, "Dynamics of the ion energy spectrum in EUV-induced hydrogen plasma," *Plasma Phys. Rep.* **43**, 614–620 (2017).
- <sup>21</sup>R. M. van der Horst, E. A. Osorio, V. Y. Banine, and J. Beckers, "The influence of the EUV spectrum on plasma induced by EUV radiation in argon and hydrogen gas," *Plasma Sources Sci. Technol.* **25**, 015012 (2016).
- <sup>22</sup>R. M. van der Horst, J. Beckers, E. A. Osorio, D. I. Astakhov, W. J. Goedheer, C. J. Lee, V. V. Ivanov, V. M. Krivtsum, K. N. Koshelev, D. V. Lopaev, F. Bijkerk, and V. Y. Banine, "Exploring the electron density in plasma induced by EUV radiation: I. Experimental study in hydrogen," *J. Phys. D: Appl. Phys.* **49**, 145203 (2016).
- <sup>23</sup>D. I. Astakhov, W. J. Goedheer, C. J. Lee, V. V. Ivanov, V. M. Krivtsum, K. N. Koshelev, D. V. Lopaev, R. M. van der Horst, J. Beckers, E. A. Osorio, and F. Bijkerk, "Exploring the electron density in plasma induced by EUV radiation: II. Numerical studies in argon and hydrogen," *J. Phys. D: Appl. Phys.* **49**, 295204 (2016).
- <sup>24</sup>A. Abrikosov, V. Reshetnyak, D. I. Astakhov, A. Dolgov, O. Yakushev, D. V. Lopaev, and V. Krivtsum, "Numerical simulations based on probe measurements in EUV-induced hydrogen plasma," *Plasma Sources Sci. Technol.* **26**, 045011 (2017).
- <sup>25</sup>H. Tawara, Y. Itikawa, H. Nishimura, and M. Yoshino, "Cross sections and related data for electron collisions with hydrogen molecules and molecular ions," *J. Phys. Chem. Ref. Data* **19**, 617 (1990).
- <sup>26</sup>J. Beckers, R. M. van der Horst, E. A. Osorio, and V. Y. Banine, "Thermalization of electrons in decaying EUV-induced low pressure argon plasma," *Plasma Sources Sci. Technol.* **25**, 035010 (2016).
- <sup>27</sup>M. Lieberman and A. Lichtenberg, *MRS Bulletin*, 2nd ed. (John Wiley & Sons, Inc., New Jersey, 2005).
- <sup>28</sup>R. M. van der Horst, J. Beckers, E. A. Osorio, and V. Y. Banine, "Exploring the electron density in plasmas induced by extreme ultraviolet radiation in argon," *J. Phys. D: Appl. Phys.* **48**, 285203 (2015).
- <sup>29</sup>E. Hamers, W. van Sark, J. Bezemer, W. Goedheer, and W. van der Weg, "On the transmission function of an ion-energy and mass spectrometer," *Int. J. Mass Spectrom. Ion Processes* **173**, 91–98 (1998).
- <sup>30</sup>K. Ellmer, R. Wendt, and K. Wiesemann, "Interpretation of ion distribution functions measured by a combined energy and mass analyzer," *Int. J. Mass Spectrom.* **223–224**, 679–693 (2003).
- <sup>31</sup>D. O'Connell, R. Zorat, A. R. Ellingboe, and M. M. Turner, "Comparison of measurements and particle-in-cell simulations of ion energy distribution functions in a capacitively coupled radio-frequency discharge," *Phys. Plasmas* **14**, 103510 (2007).
- <sup>32</sup>D. A. Dahl, J. E. Delmore, and A. D. Appelans, "SIMION PC/PS2 electrostatic lens design program," *Rev. Sci. Instrum.* **61**, 607–609 (1990).
- <sup>33</sup>H. Singh, J. W. Coburn, and D. B. Graves, "Appearance potential mass spectrometry: Discrimination of dissociative ionization products," *J. Vac. Sci. Technol. A* **18**, 299 (2000).
- <sup>34</sup>Y. M. Chung, E.-M. Lee, T. Masuoka, and J. A. R. Samson, "Dissociative photoionization of H<sub>2</sub> from 18 to 124 eV," *J. Chem. Phys.* **99**, 885 (1993).
- <sup>35</sup>J.-S. Yoon, M.-Y. Song, J.-M. Han, S. H. Hwang, W.-S. Chang, B. Lee, and Y. Itikawa, "Cross sections for electron collisions with hydrogen molecules," *J. Phys. Chem. Ref. Data* **37**, 913–931 (2008).
- <sup>36</sup>T. Tabata and T. Shirai, "Analytic cross sections for collisions of H<sup>+</sup>, H<sub>2</sub><sup>+</sup>, H<sub>3</sub><sup>+</sup>, H, H<sub>2</sub>, and H<sup>-</sup> with hydrogen molecules," *At. Data Nucl. Data Tables* **76**, 1–25 (2000).
- <sup>37</sup>J. Berkowitz, *Atomic and Molecular Photoabsorption: Absolute Partial Cross Sections* (Elsevier Science, 2015).
- <sup>38</sup>K. E. McCulloh and H. M. Rosenstock, "Experimental test of the Franck-Condon principle: Double ionization of molecular hydrogen," *J. Chem. Phys.* **48**, 2084–2089 (1968).
- <sup>39</sup>G. Dujardin, M. J. Besnard, L. Hellner, and Y. Malinovitch, "Double photoionization of H<sub>2</sub>: An experimental test of electronic-correlation models in molecules," *Phys. Rev. A* **35**, 5012–5019 (1987).
- <sup>40</sup>G. H. Dunn and L. J. Kieffer, "Dissociative ionization of H<sub>2</sub>: A study of angular distributions and energy distributions of resultant fast protons," *Phys. Rev.* **132**, 2109 (1963).
- <sup>41</sup>D. Rapp, P. Englander-Golden, and D. D. Briglia, "Cross sections for dissociative ionization of molecules by electron impact," *J. Chem. Phys.* **42**, 4081 (1965).
- <sup>42</sup>R. Plašil, J. Glosk, V. Poterya, P. Kudrna, J. Ruzs, M. Tichý, and A. Pysanenko, "Advanced integrated stationary afterglow method for experimental study of recombination of processes of H<sub>3</sub><sup>+</sup> and D<sub>3</sub><sup>+</sup> ions with electrons," *Int. J. Mass Spectrom.* **218**, 105–130 (2002).
- <sup>43</sup>S. Strathdee and R. Browning, "Dissociative photoionization of H<sub>2</sub> at 26.9 eV," *J. Phys. B: At. Mol. Phys.* **9**, L505 (1976).
- <sup>44</sup>R. W. Coons, S. S. Harilal, D. Campos, and A. Hassanein, "Analysis of atomic and ion debris features of laser-produced Sn and Li plasmas," *J. Appl. Phys.* **108**, 063306 (2010).
- <sup>45</sup>*Sputtering by Particle Bombardment*, Topics in Applied Physics Vol. 110, edited by R. Behrisch and W. Eckstein (Springer-Verlag, Berlin, Heidelberg, 2007).